Research Inventy: International Journal of Engineering And Science
Vol.11, Issue 10 (October 2021), PP 08-19
Issn (e): 2278-4721, Issn (p):2319-6483, www.researchinventy.com

Performance Evaluation of a Microstrip Wearable Antenna considering On-Body Curvature

Rafael Saraiva Campos[1]and Felipe da Rocha Henriques[2]
[1]*Department of Computer Engineering, CEFET/RJ, Petrópolis, RJ, Brazil.*
[2] *PPGIO, PPCIC, Telecommunications Department, CEFET/RJ, Petrópolis, RJ, Brazil.*
Corresponding Author: rafael.campos@cefet-rj.br

Abstract:*This work evaluates the effects of the mechanical curvature imposed on a textile inset-fedmicrostrip patch antenna positioned over a human head phantom, simulating a typical situation in WirelessBody Area Network (WBAN) applications. Initially, the antenna geometrical parameters are defined underideal free-space conditions, assuming a 5.8 GHz centre frequency. Following, this work assesses theeffects of body proximity and antenna curvature on operational characteristics, such as resonant frequency,bandwidth, and radiation pattern. The antenna design and evaluation employs finite-element method models.Most of the antenna geometrical parameters are analytically defined, but some are obtained using Nelder-Mead optimization. Furthermore, the resulting Specific Absorption Rate on the head is calculated andcompared with international safety standards. Computational results show that the curvature of the antenna,when placed on the human head, causes a relevant shift on resonant frequency. Thereby, the initial antenna design must provide a sufficiently large bandwidth to account for such detrimental effect. Accordingly, theproposed antenna reached 790 MHz bandwidth (at the expenses of a thicker substrate), which ensures properoperation when applied over the body in WBAN applications. The designed antenna also yielded a 19 dBfront-to-back ratio, minimizing brain radiation exposure.*

Keywords:*Wireless Body Area Network, health monitoring, microstrip antenna, specific absorption rate, Nelder-Mead optimization.*

Date of Submission: 02-11-2021 Date of Acceptance: 18-11-2021

I. INTRODUCTION

Wireless Sensor Networks(WSNs) are ad hoc networks composed by sensor nodes capable of monitoring given areas of interest[1]. This work lies within the context of a specificapplication of WSNs, referred to as Wireless Body Area Networks(WBANs), in which the nodes aim to collect biometric data from patients, such as electrocardiogram(ECG), electroencephalogram(EEG), or glucose data[2]. WBAN sensors usually are placed on the patient's body or implanted under their skin. Despite the sensors low transmission power,their close proximity to the human body raises concerns regarding electromagnetic radiation exposure[3].

Microstrip antennas are low cost, light in weight, have a low profile and thereby can be integrated into printed circuits. These characteristics make them preferred choicesfor WBAN related applications. However, there are two main drawbacks associated with these antennas: high input impedance and narrow bandwidth. The former issue can beaverted by using the inset-fed technique, where the amount of inset of the feed line controls the antenna input impedance. The latter can be solved increasing the dielectric substrate height [4].

This work addresses the problem of designing a textile inset-fed microstrip patch antenna, operating in the WBAN at the central frequency of 5.8 GHz, which lies within theFederal Communications Commission (FCC) allotted band for the operation of Ultra-Wide Band (UWB) signals [5]. However, its main contribution is the assessment of wearableantenna electromagnetic parameters, such as isotropic gain, impedance bandwidth, resonant frequency, and reflection coefficient, when it is applied over an on-the-body curvedsurface, such as the human head. Moreover, the resulting Specific Absorption Rate (SAR) at the human head and brain models is calculated, in order to verify compliance withthe International Commission on Non-Ionizing Radiation Protection (ICNIRP) guidelines [6]. To achieve the aforementioned goals, finite-element method (FEM) simulation models are set-up using COMSOL Multiphysics software.

The placement of the textile antenna on the head considers specific situations within health monitoring, such as remote access electroencephalogram (EEG) [7], where placing the antenna in other part of the body would require long wires connecting the electrodes (placed on the head) and the antenna, or tumour detection through microwave brain imaging system [8] [9], in which the antenna must be placed on the head.

Several published papers evaluate the effect of bending inwearable textile antenna performance, but not as many evaluate the SAR inside the wearer's body [10] [11] [12] [13][14] [15] [16], or, more specifically, into his head and brain.Measuring the SAR inside the head, and particularly, insidethe brain, is of course difficult and not recommended. Thus,one relies mostly on simulations for such analysis.

In [13], the authors evaluate the performance of a wearabletextile antenna when subjected to different bending radii.The antenna is designed to operate around 4 GHz. Theantenna is placed on the torso and right arm of the testsubject. The authors reported that the radiation pattern andimpedance matching in proximity of a human body and undermechanical bending remain stable.

In [14], the authors assess the performance of a textile antenna subjected to different bending curvatures, andalso evaluate its electrical parameters under distinct statesof wetness (inside water, wet, approximately dried, completely dried). Bending and wet performances for Ultra-WideBand (UWB) reception using wearable textile antennas isalso evaluated through simulations in [15]. No considerationregarding body proximity is made in both papers.

In [16] the authors design and evaluate a flexible patchUWB antenna for WBAN communication using differentsubstrates: felt and Rogers RO4350B ceramic. Their simulations indicate a 30% reduction in bandwidth of the antennawith RO4350B substrate, when it is bent with a curvatureradius of 80 mm. The bandwidth of the antenna using feltas substrate increased when bent with a curvature radius of40 mm, but at the expense of a poorer S_{11} and lower resonantfrequency. Again, the effect of body proximity on antenna performance is not considered.

In [17] the authors study the performance of a textile microstrip patch antenna when placed over a curved surface (theleft arm) over the body. The antenna bandwidth and the SARinside the arm are evaluated for curvatures of 40°, 60°, and 90°. The authors used a FEM model in the simulations.

In [18], the authors evaluate the SAR by placing the antenna at different distances from the body and using differentpolarizations. The effect of bending on antenna performanceis not assessed, but the effect of body proximity is: theauthors use a cylindrical phantom model to represent thestructure of the human body in the simulation. Their resultsindicated that the SAR is maximized when the wearabletextile antenna is horizontally polarized. Their simulationuses the Finite Integration Technique (FIT). As FEM, FITis a spatial discretization scheme to numerically solve electromagnetic field problems [19].

II. EXPERIMENTAL PROCEDURE

2.1. Dielectric Materials and Human Head Phantom

The wearable antenna substrate must be fully flexible, sojeans fabric, a cheap and readily available textile material,is used. Thin copper sheets compose the antenna conductingsurfaces (patch, microstrip and ground-plane).

The human head phantom imported into the FEM modelfollows the IEEE specifications for simulations of exposureto non-ionizing radiation [20]. The head geometry is scaleddown to 60% of its original size, which yields a head modelcompatible to that of a human newborn. An ellipsoid withinthe skull represents the brain [21]. Figure 1 illustratesthe head phantom and the simplified brain model inside of it.

The aforementioned scaling down is carried out to reducethe number of elements (and therefore degrees of freedom)in the FEM spatial discretization. This may be a concern, interms of hardware requirements for the simulations, as thesenumber might be extremely high.

Both the brain and the skull are assumed to be homogeneousand isotropic. The dielectric properties of the headphantom are that of cortical bone tissue.

Table 1informs the dielectric constant (ε_r), conductivity (σ) and mass density(ρ) of the materials used in the FEM models. The mass densities of the brain and the head are required to calculate the SAR at those regions.

Table 1. Materials Properties at 5.8 GHz.

Material	ε_r	σ (S/m)	ρ (kg/m^3)	References
Jeans	1.78	0.04882	-	[22]
Copper	1	5.8×10^7	-	[22]
Air	1	0	-	[23]
Brain	44	4.99	1046	[23],[24]
Head	9.67	1.15	1908	[23],[24]

Figure 1 - Side and top view of the human head phantom and simplified brain model.Parts of the head surface have been omitted to allow visualization of its interior.

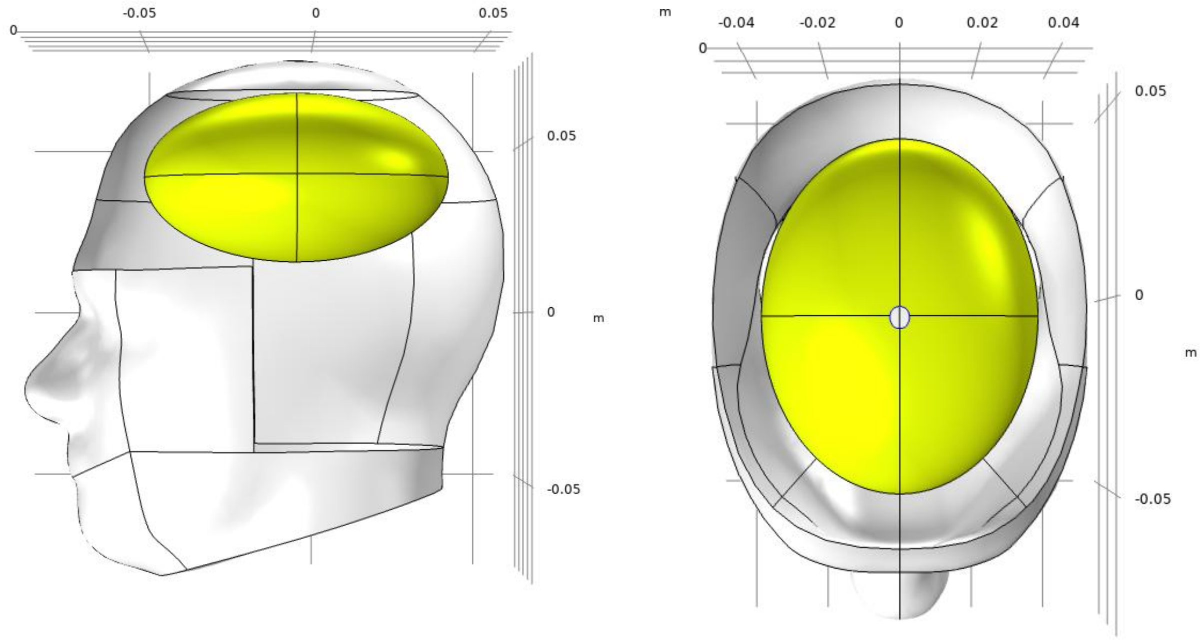

2.2. Antenna Design

Figure 2 shows the configurable antenna geometric parameters. Table 2 brings their descriptions and selected values for the 5.8 GHz centre frequency. The patch and ground plane were modelled as Perfect Electric Conductor (PEC) surfaces, as copper skin depth at 5.8 GHz is δ = 0:86 m, and $\delta \ll$ h. The values of L, W, L_g, W_g, S_i, and L_f were defined using analytical expressions. Firstly, the initial value of W is given by:

$$W = \frac{\lambda}{2}\sqrt{\frac{2}{\varepsilon_r + 1}} \tag{1}$$

where ε_r is the relative electrical permittivity in Farads per meter (also known as dielectric constant) of the dielectric substrate, and λ is the wavelength (meters) in free space at the antenna resonant frequency [25]. Following, parameter L is defined by:

$$L = \frac{\lambda}{2\sqrt{\varepsilon_{\text{eff}}}} - 2\Delta L \tag{2}$$

where ε_{eff} is the effective dielectric constant [26] and ΔLis the length normalized extension [27], which accounts forthe fact that, due to fringing effect at the borders, electricallythe microstrip patch seems longer than its physical dimension[31]. Parameters ε_{eff} and ΔL are specified by

$$\varepsilon_{\text{eff}} = \frac{\varepsilon_r + 1}{2} + \frac{\varepsilon_r - 1}{2\sqrt{1 + 12\frac{h}{W}}} \tag{3}$$

$$\Delta L = 0.412h\left[\frac{\varepsilon_{\text{eff}} + 0.3}{\varepsilon_{\text{eff}} - 0.258}\right]\left[\frac{\frac{W}{h} + 0.264}{\frac{W}{h} + 0.813}\right] \tag{4}$$

Following, the substrate planar dimensions are defined as L_g = 2L and W_g = 2W. The patch inset length is provided by [27]:

$$S_i = \frac{L}{\pi} \arccos\left(\sqrt{\frac{Z_0}{R_{in}}}\right) \tag{5}$$

where Z_0 is the feed line input impedance, and Rin is the real part of the antenna input impedance, given by:

$$R_{in} = \frac{1}{G_{11} + G_{12}} \tag{6}$$

where G_{11} is the conductance of a single slot in the antenna equivalent circuit, and G_{12} is the mutual conductance of the two slots in the antenna equivalent circuit. These two parameters are given by

$$G_{11} = \frac{1}{90}\left(\frac{W}{\lambda}\right)^2 \tag{7}$$

$$G_{12} = \frac{1}{120\pi^2} \int_0^{\pi} J_0\left(x\right) \sin^3\theta \left[f\left(W, \lambda, \theta\right)\right]^2 d\theta \tag{8}$$

where

$$x = \frac{2\pi}{\lambda} L \sin\theta \tag{9}$$

$$f\left(W, \lambda, \theta\right) = \frac{\sin\left(\frac{W\pi\cos\theta}{\lambda}\right)}{\cos\theta} \tag{10}$$

and J_0 is the zero order Bessel function of the first kind.Finally, the line feed length is obtained from:

$$L_f = \frac{L_g - L}{2} + S_i - S_0 \tag{11}$$

The values of S_g, W_f and S_0 were set using Nelder-Meadoptimization [28], submitted to the following restrictions: 100 μm ≤ S_g≤ 2000 μm, 3 mm ≤ W_f≤ 8 mm, 0.1 mm ≤ S_0≤ 6 mm. The initial values of S_g, W_f and S_0 are 200 μm, 5.68 mm, and 1.34 mm, respectively. Theobjective function (to be minimized) is the S_{11} parameter.The value of *h* was manually adjusted in order to increasethe antenna bandwidth.

Figure 2. Patch antenna geometric parameters

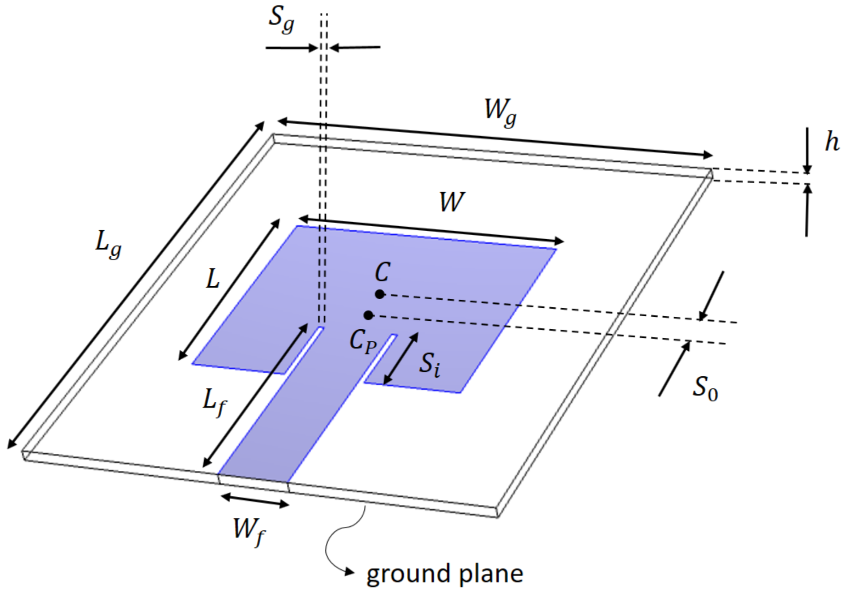

2.3. Nelder-Mead Optimization

The Nelder-Mead method (NMM) is a simplex-based directsearchalgorithm to optimize scalar functions. Direct-searchmethods are based on comparison of function values only,thereby do not need any information on function derivatives,neither analytical nor numerical. This represents an advantageof NMM: the objective function does not need to bedifferentiable, as is the case in gradient-descent methods, norcontinuous [28].

The basic element of the NMM is the simplex, which isa convex hull in formed by n + 1 points (vertices). Duringthe execution of the algorithm, the simplex changes its form,orientation and position, following a set of rules. The algorithmhalts after 1000 iterations. The sub-optimal solution isprovided by the centroid of the simplex in the last iteration.

NMM is a downhill simplex method, thus it moves onlydownhill. As a result, the algorithm can get stuck in alocal minimum providing a poor solution. An alternativeto circumvent that is to perturb the current simple withrandom noise and start again (NMM+perturbations). Anotheralternative is to combine NMM with simulated annealing,to allow hill climbing [29]. There are also some problemsregarding NMM convergence [30].

Despite the aforementioned issues, NMM has the advantageof being suitable to optimize non-differentiable functions,and it has proven to work very well in practice. Infact, in the problem addressed in this paper, i.e., S_{11} optimization,NMM has succeeded where Levenberg-Marquardtand Monte Carlo simulation have failed.

2.4. First Simulation Scenario

In the first scenario, the antenna design is validated underideal circumstances (free space). As Figure 3 shows, theantenna is placed at the centre of a spherical Perfect MatchingLayer (PML), emulating the conditions inside an anechoicchamber.

As previously stated, the values of S_g, W_f, and S_0 areoptimized using Nelder-Mead simplex method, in order tominimize reflections at the input port, and all remaininggeometric parameters are analytically defined. The antennais fed using a lumped port at the edge of the microstrip, withZ_0 = 50 ohms input impedance and 1 Volt.

In order to reduce computational cost, it is necessary tolimit the number of tetrahedron-shaped finite elements in theFEM model mesh. However, this must be carried out withoutperceptively degrading the model resolution or impairing theconvergence of the simulation. Thereby, the minimum andmaximum finite element sizes were set to $\lambda/10$ and $\lambda/3$, respectively, where λ = 5.1 cm is the wavelength at 5.8 GHz.During the mesh generation, the element size starts with theminimum value at boundaries and edges, and increases with a maximum growth rate of 1.5 per layer as one moves awayfrom such regions. This resulted in a mesh containing 45258tetrahedral elements and 304750 degrees of freedom. Figure 4 illustrates a region of the variable element-size meshgenerated as previously described.

Figure 3. First Simulation Scenario

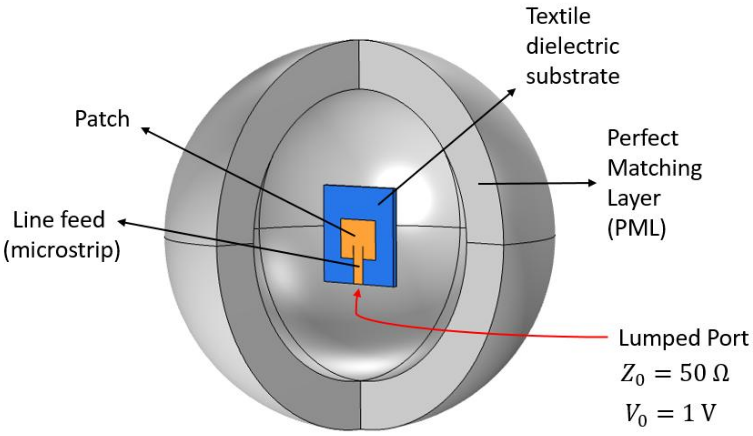

Figure 4. Detail of the variable element size mesh used in the discretization of the FEM model. The section displayed in the figure comprises the antenna patch, microstrip, feed line and a part of the upper surface of the dielectric substrate. Note the higher detail at the two feed line insets. The smaller element size at areas with finer detail ensures a more accurate simulation

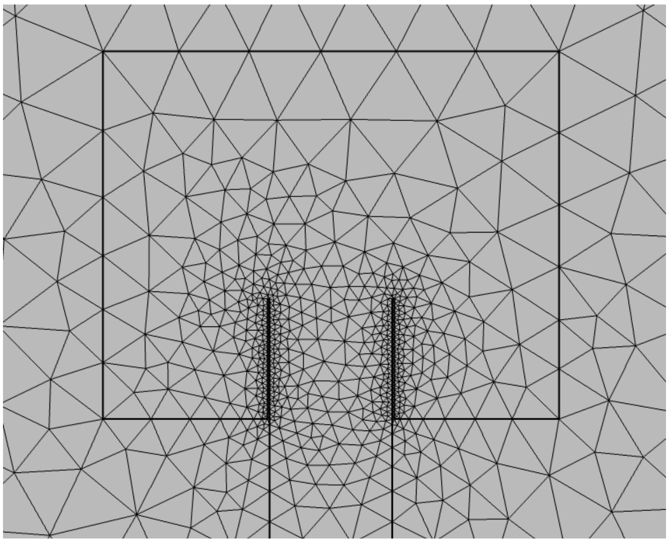

2.5. Second Simulation Scenario

In the second scenario, the textile antenna designed in thefirst scenario is positioned over the human phantom head. The antenna is placed over the skullleft parietal region, as Figure 5(a) illustrates. This results in a bend angle θ = 49.5°, as Figure 5(b) shows.

Following, the FEM model is excited by frequencies rangingfrom 5 to 7 GHz, with a 10 MHz step. During thisfrequency sweep, the response of the model is computed,allowing to obtain the coefficient of reflection, as well as theradiation patterns, at each frequency.

The addition of the human head phantom, as well as ofthe brain model, results in a dramatic increase in the numberof finite elements (and thereby degrees of freedom) in themodel, in comparison to the first scenario. The mesh ofthe FEM model is generated just like in the first scenario.Therefore, the number of elements varies with frequencyduring the frequency sweep, as the minimum and maximumelement sizes are functions of the wavelength. Consequently,the number of elements ranges from 257571 (at 5 GHz)to 599265 (at 7 GHz). At the highest frequency, the FEMmodel has 3715566 degrees of freedom.

Figure 5. (a) Human head phantom with part of its surface hidden to allow visualization of the brain model (yellow ellipsoid); (b) Curvature of the antenna placed over the head.

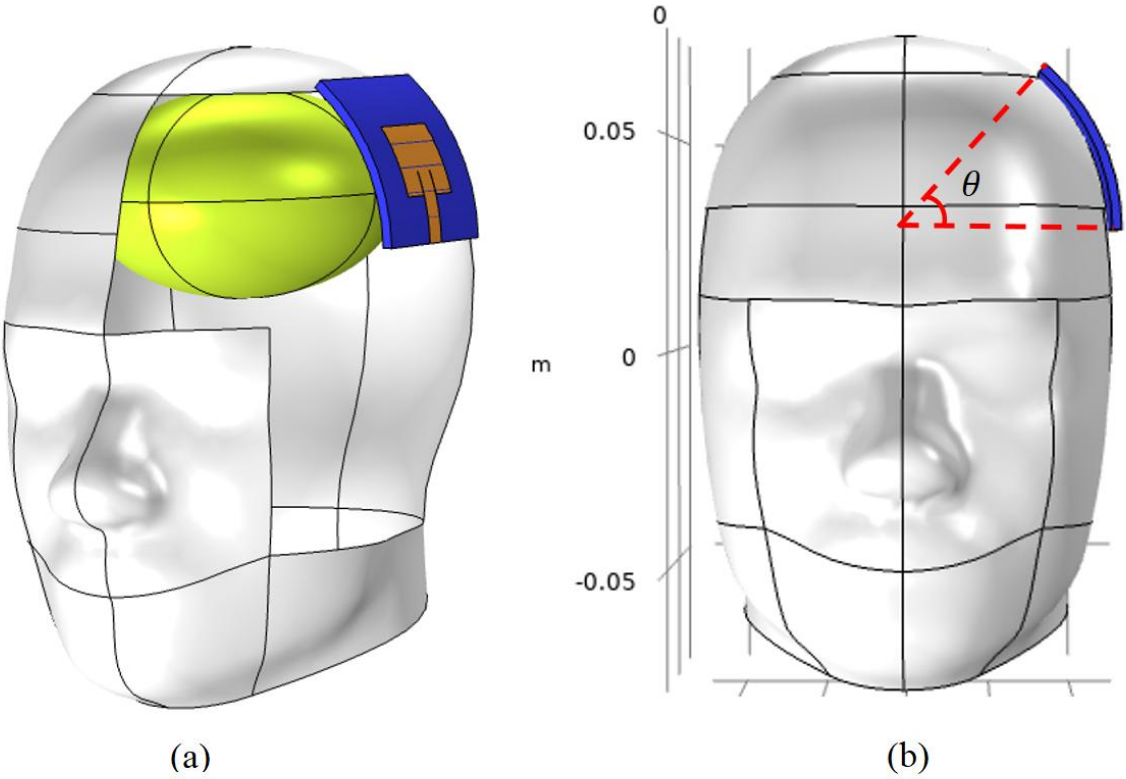

III. RESULTS AND DISCUSSIONS

3.1. Bandwidth

Figure 6 shows the coefficient of reflection (S_{11}) as a functionof frequency in the two simulated scenarios. The curve forthe first scenario (in blue) indicates that the antenna wassuccessfully fined tuned to operate at the 5.8 GHz centralfrequency, with a -10 dB return loss bandwidth of 790 MHz.The curve for the second scenario (in red) informs that theresonant frequency shifts from 5.8 GHz to 5.67 GHz, andthat the -10 dB return loss bandwidth diminishes from 790MHz (5.43 - 6:22 GHz) to 660 MHz (5.34 - 6 GHz). Thisyields a 400 MHz band centred at the originally designedresonant frequency, i.e., 5.8 GHz. Such bandwidth is morethan enough to accommodate the expected data rates intypical mobile health applications, as Table 3 indicates.

Table 3. Bit Rate Requirements for WBAN Health MonitoringApplications [5].

Application	Bit Rate (kbps)
Glucose Level Monitor	1
EEG (electroencephalogram)	86.4
ECG (electrocardiogram)	192
Deep brain stimulation	320
Endoscopy through capsule	1000

Figure 6. Coefficient of reflection as a function of frequency for bothsimulated conditions (plane antenna in free space and curved antenna overthe head).

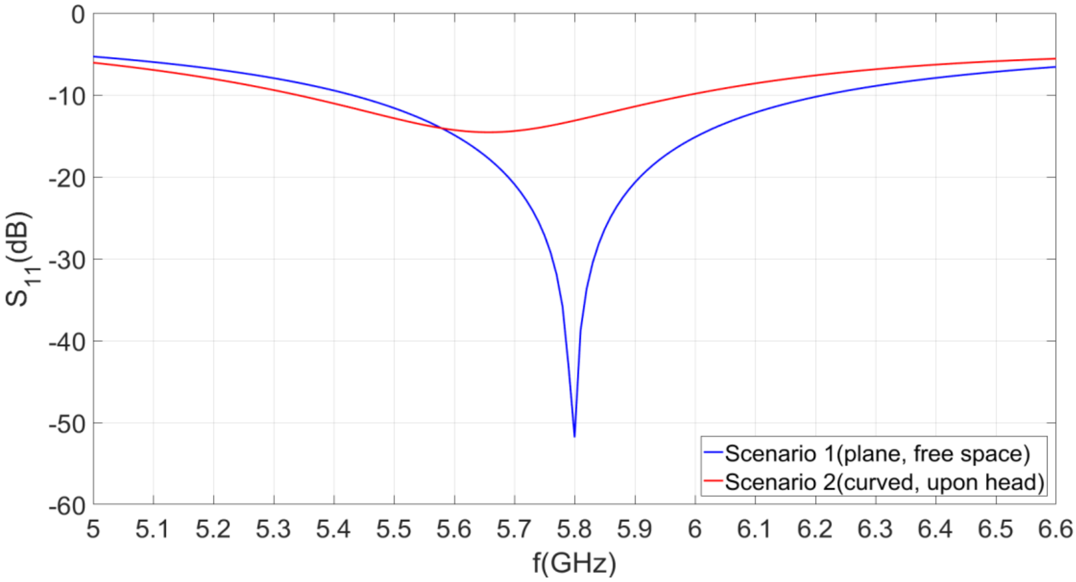

3.2. Radiation Pattern and Isotropic Gain

Figure7 shows that the antenna curvature and presenceof the head do not significantly affect the -3 dBbeamwidth (which falls from 65 to 58 degrees) neither thefront-to-back ratio (which increases from 19 to 23 dB).The front-to-back ratio as high as 23 dB shows that theantenna radiation pattern is directed away from the person,which results both in less power being uselessly dissipated inthe body, as well as in lower radiation exposure.The antenna isotropic gain in both scenarios remainsaround 4 dB.

Figure 7. (a) Horizontal and (b) vertical radiation patterns at 5.8 GHz of undeformed antenna in free space (blue) and of curved antenna over the head (red).

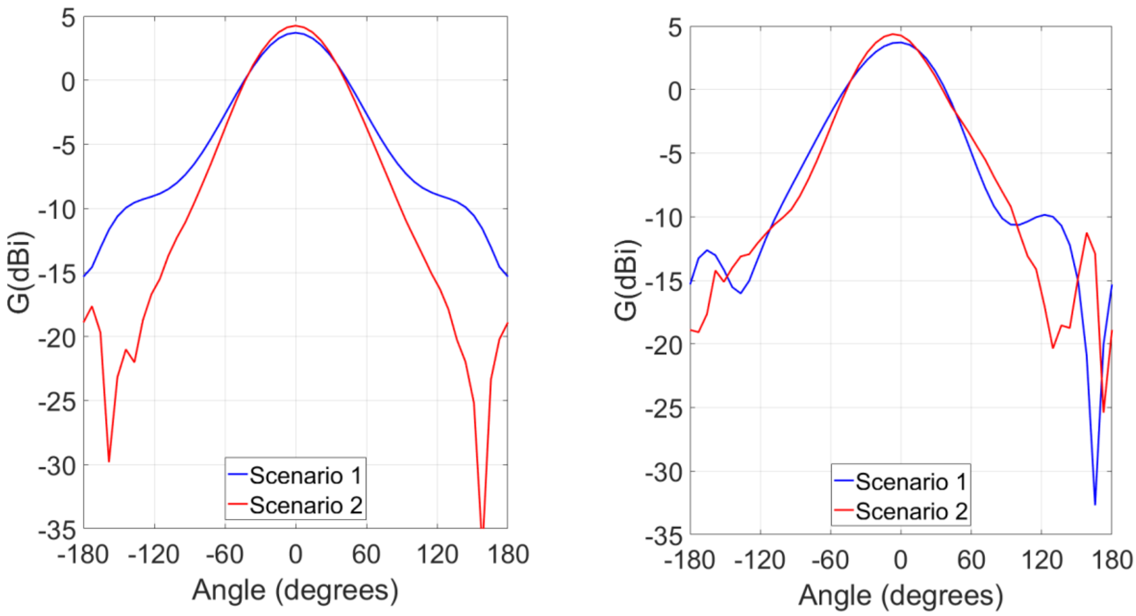

These results suggest that the wearable inset-fed microstrip patch antennadesigned in this work preserves its operational capabilities(with regard to WBAN applications) at the intendedresonant frequency of 5.8 GHz.

3.3. SAR and Compliance with ICNIRP Safety Regulations

Figure 8 shows the electric field intensity, which is markedlymore intense at the microstrip and patch borders, due to thefringing effect. Following, Figures 9 and 10depicts the SARover the surface and inside the head phantom, respectively.The SAR values are expressed in logarithmic scale for improvedvisualization. In Figure 10 the top section of the humanhead phantom is clipped, so that the SAR inside the headand the brain can be seen. The highest value occurred at theouter surface of the head, next to the antenna feeding point, and was equal to 0.955 W/Kg. The highest SAR value insidethe simplified brain model was 0.01 W/kg (see Figure 11).Those values correspond to 47.5% and 0.5%, respectively,of the ICNIRP general public maximum recommended localSAR in the head and torso (2 W/Kg) [6].

Figure 8. Electric field intensity (V/m). The picture shows both the head phantom and the spherical PML used in the simulation. For simplicity, the former is omitted from the next figures.

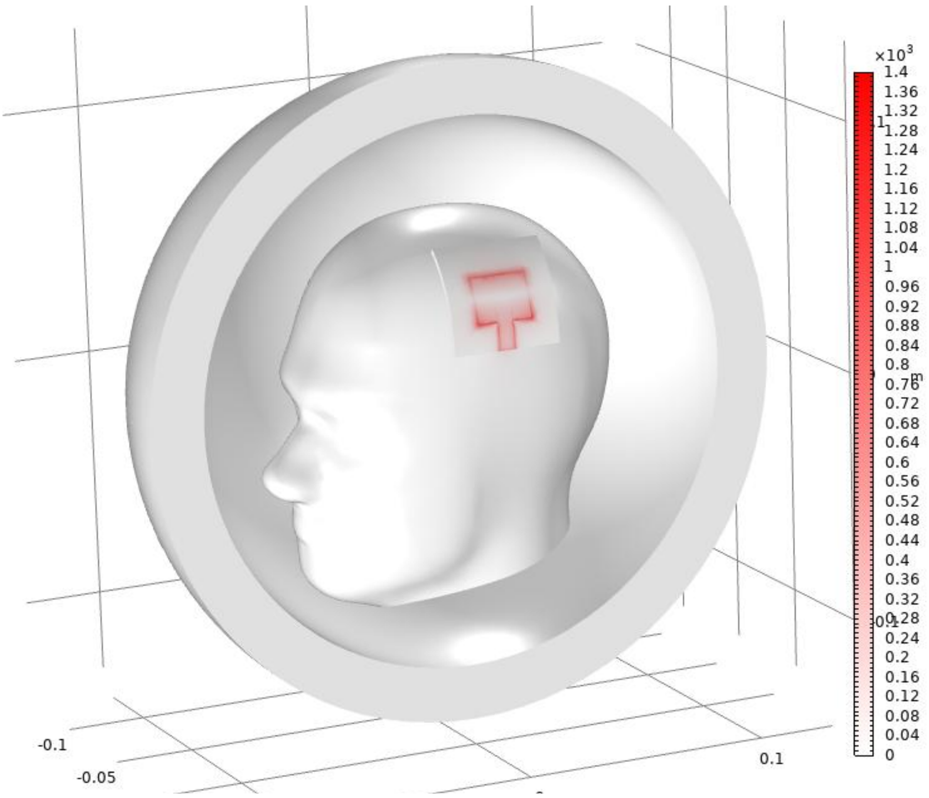

IV. CONCLUSION

The FEM simulation results indicate that the proposed textilemicrostrip patch antenna is suitable - both from the radiofrequencyand health safety standpoints - for on-the-bodydeployment in the context of WBAN applications for healthmonitoring. Future developments of this work concentrate on (1) improving simulation accuracy through the use ofmulti-layered head and brain models that take intoaccount the non-uniformity of such regions and alsobetter represent the brain morphology; (2) evaluating evolutionary based optimization, such asGenetic Algorithms; (3) manufacturing and testing the proposed antenna in areal scenario.

Conflict of interest

There is no conflict to disclose.

Figure 9. SAR (in log scale) on the human head phantom surface

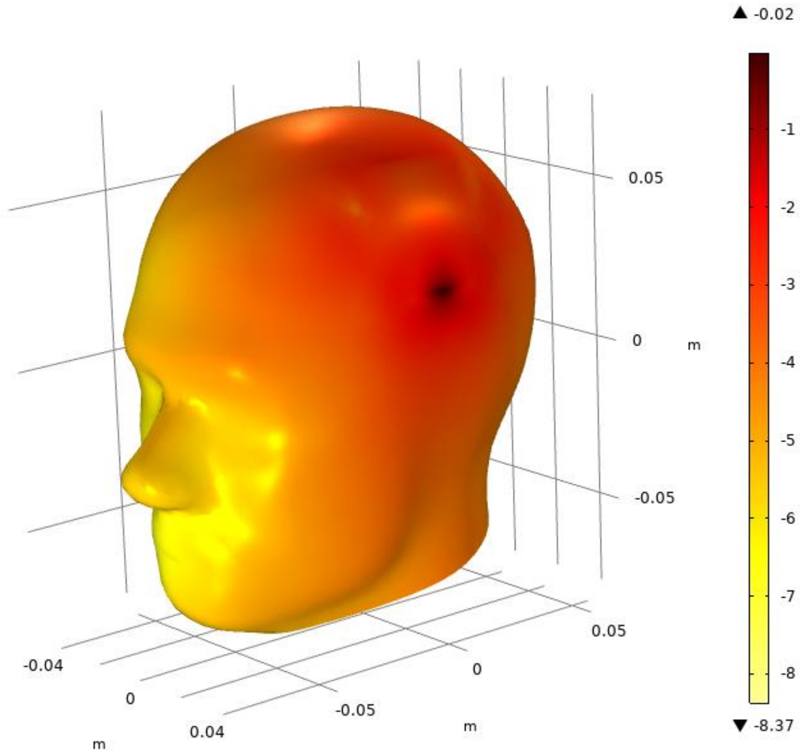

Figure 10. SAR (in log scale) inside the human head phantom surface

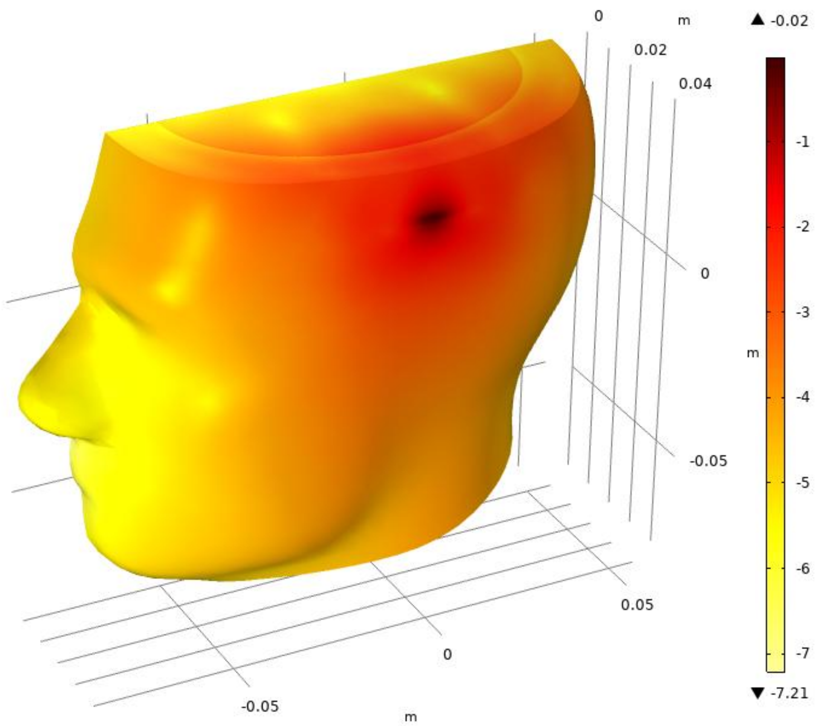

Figure 11. SAR (in log scale) inside the simplified brain model.

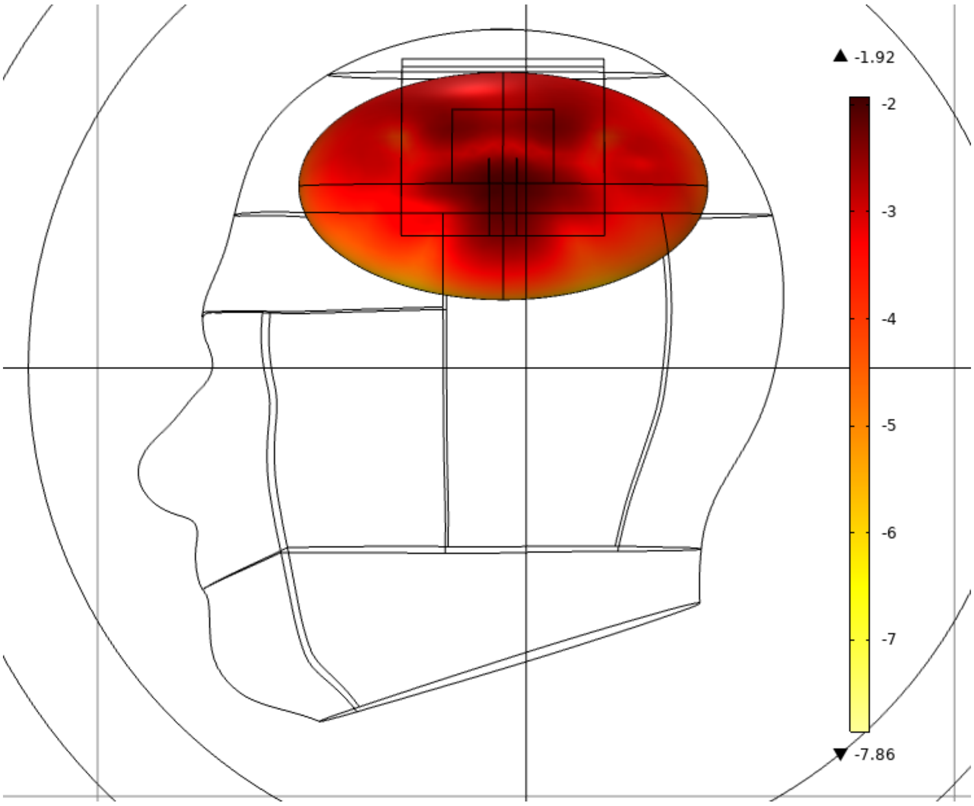

REFERENCES

[1]. F. Akyildiz, W. Su, Y. Sankarasubramaniam, and E. Cayirc, "Wireless Sensor Networks: A Survey," Computer Networks, vol. 38, no. 4, pp. 393–422, March 2002.

[2]. D. O'Hare, "Biosensors and Sensor Systems," in Body Sensor Networks, G. Yang(Editor), 1st Ed., London, Springer, 2008, pp.55–115.

[3]. G. Ahmed et al., "Rigorous Analysis and Evaluation of Specific Absorption Rate (SAR) for Mobile Multimedia Healthcare," IEEE Access, vol.6, pp. 1–9, May 2018.

[4]. N.J. Kolias, R.C. Compton, J. Patrick Fitch, and David M. Pozar, "Microstrip Antennas," in The Electrical Engineering Handbook, R. C. Dorf (Editor), 2nd Ed., Boca Raton, Florida, CRC Press, 2000, Ch.38, pp. 1012–1020.

[5]. V. C. Ferreira, H. Balbi, F. L. Seixas, C. Albuquerque, and D. C. Muchaluat–Saade, "Wireless Body Area Networks: Na Overview," in XXXV Simpósio Brasileiro de Telecomunicações e Processamento de Sinais–SBrT 2017, São Pedro, Brazil, 2017, pp. 1–14.

[6]. International Commission on Non-Ionizing Radiation Protection, "ICNIRP Guidelines for Limiting Exposure to Electromagnetic Fields (100 KHz TO 300 GHz)," Health Physics, vol. 118, no.5, pp. 483–524, May 2020.

[7]. Bittium Corporation, "Bittium BrainStatus™ Wireless EEG Amplifier" [Online]. Available: https://www.bittium.com/medical/bittium-brainstatus, Acessed on: October,2,2021.

[8]. R. Inum, Md. M. Rana, and Md. A. Quader, "Modeling of an efficient microstrip patch antenna for microwave brain imaging system," in 2016 3rd International Conference on Electrical Engineering and Information Communication Technology (ICEEICT), Dhaka, Bangladesh, 2016, pp.1–6.

[9]. R. Inum, Md. M. Rana, K. N. Shushama, and Md. A. Quader, "EBG Based Microstrip Patch Antenna for Brain Tumor Detection via Scattering Parameters in Microwave Imaging System," International Journal of Biomedical Imaging, vol. 2018, Article ID 8241438, 12 pages, 2018.

[10]. S. R. Zharan, M. A. Abdalla, and A. Gaafar, "How Bending Affects a Flexible UWB Antenna,", Microwaves & RF [Online]. Available: //www.mwrf.com/technologies/passivecomponents/article/21847050/how-bending-affects-a-flexible-uwbantenna, Accessed on: October,4,2021.

[11]. K. Saraswat and A. R. Harish, "Flexible dual-band dual-polarised CPW fed monopole antenna with discrete-frequency reconfigurability,", IET Microwaves, Antennas & Propagation, vol.13, no.12, pp.2053—2060, July, 2019.

[12]. Y. Jiang et al., "e-Textile embroidered wearable near-field communication RFID antennas,", IET Microwaves, Antennas & Propagation, vol.13, pp.99–104, October, 2018.

[13]. D. V. Baelen, Q. V. Brande, S, Lemey, J Verhaevert, and H. Rogier, "Foldable All-Textile Cavity-Backed Slot Antennas for Personal UWB Localization," Radio Science, 55, e2019RS006990, February 2020.

[14]. M. A. R. Osman, M. K. A. Rahim, N. A. Samsuri, M. K. Elbasheer, and M. E. Ali, "Textile UWB Antenna Bending and Wet Performances," International Journal of Antennas and Propagation, vol. 2012, Article ID 251682, pp. 1–12, March 2012.

[15]. M. S. Shakhirul, M. Jusoh, A. Sahadah, C. M. Nor, and H. A. Rahim, "Embroidered wearable textile antenna on bending and wet performances for UWB reception," Microwave and Optical Technology Letters, vol. 56, no.9, pp. 2158–2163, September 2014.

[16]. S. Kassim et al., "Flexible Co-Planar Waveguide (CPW)-Fed Y-Shaped Patch UWB Antenna for Off-Body Communication," Journal of Physics: Conference Series, vol. 1464, no.012058, 2020.

[17]. E. Freitas, L. Queiroz, J. Silva, and S. Holanda, "Análise do desempenho de antena têxtil em superfícies curvas para aplicação em WBAN," (in Portuguese) in XXXVIII Simpósio Brasileiro de Telecomunicações e Processamento de Sinais (SBrt 2020), Florianopolis, Brazil, 2020, pp.1–5.
[18]. H. H. Zainal et al., "SR Evaluation of Metallic Loop-like Accessory Effect of Broadband Wearable Planar Monopole Textile Antenna," Advanced Electromagnetics, vol.7, no.3, pp. 17–22, August 2018.
[19]. A. Demenko, J. K. Sykulski, and R. Wojciechowski,"On the Equivalence of Finite Element and Finite Integration Formulations," IEEE Transactionson Magnetics, vol.46, no.8, pp. 3169–3172, August 2010.

Rafael Saraiva Campos, et. al. "Performance Evaluation of a Microstrip Wearable Antenna considering On-Body Curvature." *International Journal of Engineering and Science*, vol. 11, no. 10, 2021, pp. 08-19.